Macromolecules

ARTICLE

pubs.acs.org/Macromolecules

Effect of Solvent Evaporation Rate on Order-to-Disorder Phase Transition Behavior of Regioregular Poly(3-butylthiophene)

Yuan Yuan, Jianming Zhang,* and Jiaqian Sun

Key Laboratory of Rubber-Plastics, Ministry of Education/Shandong Provincial Key Laboratory of Rubber-plastics, Qingdao University of Science & Technology, Qingdao City 266042, People's Republic of China

ABSTRACT: The effect of solvent evaporation rate on the crystal modification and the thermal stability of solution cast regioregular poly(3-butylthiophene) (P3BT) film was investigated by WAXD, DSC, and FTIR. It is found that, independent of the solvent evaporation rates, the P3BT films prepared from chloroform solution demonstrate essentially the same interlayer distance, which is very close to the reported value of form I′, rather than the conventional form I. However, in the DSC heating curves, it is interesting to find that a single "melting" peak and a double one in the temperature region of 45−100 °C can be observed respectively for P3BT films prepared with fast and extremely slow solvent evaporation rates. The double melting behavior of P3BT in this low-temperature region has never been discussed in the literature. By temperature-dependent infrared spectroscopy, it is shown that these low-temperature "melting" peaks are related to the order-to-disorder phase transition (form I′ to form I) of P3BT. Furthermore, our spectral studies reveal that the "melting" peak around 58 °C in the DSC heating trace is associated with the conformational disordering of butyl side chains, whereas the destruction of backbone planarity and the disordering of $\pi-\pi$ stacking can take place at higher temperature (ca. 82 °C) with decreasing the solvent evaporation rate.

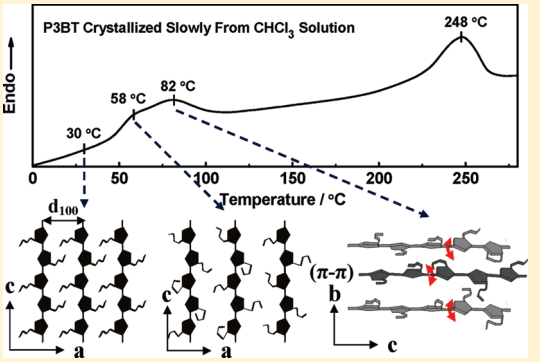

1. INTRODUCTION

Poly(3-alkylthiophene) (P3AT) is thought to be one of the most economical and promising conjugated polymers, which have many potential applications such as field-effect transistors (FETs), organic photovoltaic cells (OPVs), and so on.[1,2] A major element of the extensive interest attracted to this kind of conductive polymer derives from the fact that it can be prepared via solvent-based technology which ensures that the fabrication cost remains low and the processing is simple.[3−5] What should be noticed is that most of the research is focused on poly(3-hexylthiophene) (P3HT) due to P3HT possesses excellent solution processability and high field-effect mobility,[6−8] whereas relevant work on poly(3-butylthiophene) (P3BT, see Scheme 1 for its chemical structure) is less during the past decade. However, because P3BT has the shorter butyl side chains, it is suitable to be used as the model to understand the crystal structure of P3AT. Moreover, the higher crystallinity of P3BT gives the chance to this conjugated polymer in the application of photovoltaic devices. Accordingly, P3BT has received increasingly academic and technological attention in recent years.[9−14]

As a kind of semicrystalline polymer, the properties of P3BT strongly depend on its crystalline structure and morphology in the resulted film. It has been widely accepted that, in the lamellar structure of P3BT, parallel stacks of conjugated main chains are separated by regions filled with the butyl side chains.[15,16] On the basis of this stacking mode, P3BT can be organized into two types of crystal modifications named form I and form II. In form I crystal, butyl groups of P3BT remain in the staggered conformation, and the overlapping of the side chains on the neighboring stacking is minimal.[10] In contrast, the interdigitation of side chains occurs in form II crystal, reducing the interlayer distance between adjacent backbones greatly.[10−13] According to Prosa's idea,[17] the structural models of P3BT form I and form II modifications can be depicted as those in Scheme 2. Recently, another new crystal modification of P3BT named form I′ has been identified.[14] It is reported that this new crystal form is closely related to the more common but more disordered form I of P3BT according to the X-ray diffraction data.

In general, in order to improve the structural regularity so that the charge-carrier mobility can be improved accordingly, annealing treatment between the glass transition temperature (T_g) and the melting temperature (T_m) is often performed for P3AT film.[18] However, the design of annealing procedures should be based on the temperature-dependent phase diagram because the molecular mobility and the inter- or intrachain packing modes in the various phases are largely different. Therefore, study on the phase transition behavior between various crystal modifications continues to be an important research topic of P3BT. For example, Yang et al.[19] first reported the phase transition of form I to form II upon controlled solvent vapor treatment. Subsequently, they also

Received: April 27, 2011
Revised: May 20, 2011
Published: July 05, 2011

Scheme 1. Molecular Structure of rr-P3BT

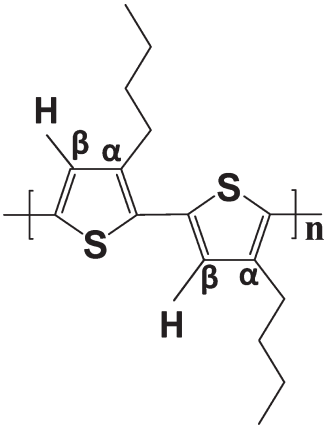

Scheme 2. Schematic Models of the Form I (a) and Form II (b) Crystal Structure for rr-P3BT

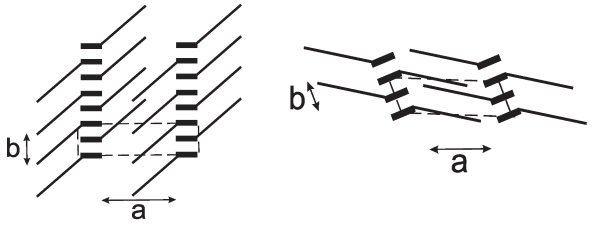

found that the form II modification can be transferred back to form I at about 159 °C via a solid−solid phase transition at elevated temperature. The authors ascribed the reason for this transition to the thermostability difference of these two modifications. Very recently, Arosio et al.[14] proposed that an endothermic peak around 60 °C observed in the DSC heating curve of their native P3BT sample may be related to the phase transition from form I′ to form I. However, the structural changes involved in this phase transition process have not been clarified yet.

It is well-known that the solvent evaporation rate plays an important role on controlling the morphology, crystallinity, and even the molecular orientation of solution cast P3AT film.[11,19−21] In this paper, by controlling the solvent evaporation rate together with the solvent vapor treatment, the crystallinity and regularity of P3BT form I′ crystal were largely improved. It is surprised to find that a double endothermic behavior rather than a single one displayed for the P3BT film prepared under extremely slow solvent evaporation rate. The origin of such double "melting" behavior in the temperature region between the glass transition temperature (T_g) and the melting point (T_m) of P3BT was investigated by temperature-dependent IR spectroscopy. Moreover, the sequence changes of butyl side chains, the effective conjugation length, and the $\pi-\pi$ stacking of P3BT in heating process are discussed. It is expected that our work could be helpful for establishing the temperature-dependent phase diagram of P3BT crystal and providing some new insights into understanding the phase transition mechanism of form I′ to form I.

Scheme 3. Schematics for the Preparation of rr-P3BT Film with Slow Solvent Evaporation Rate: (a) Casting Several Drops of P3BT/$CHCl_3$ Solution onto the Substrate, Which Is in the Jar with a Small Amount of Solvent in the Bottom; (b) P3BT Film Turns to Dry Gradually in the Solvent Atmosphere; (c) P3BT Film Was Obtained on the Substrate after ca. 24 h

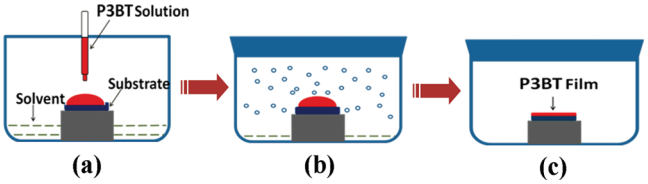

2. EXPERIMENTAL SECTION

2.1. Material and Sample Preparation Procedure. Regioregular poly(3-butylthiophene) (P3BT) (M_w = 5.48 × 10^4 g/mol and M_n = 2.21 × 10^4 g/mol, regioregularity is 93−95%) was purchased from Rieke Metals, Inc. The native sample was dissolved in chloroform (concentration 15 mg/mL) and stirred on a hot stage at 40 °C for at least 1 h. Subsequently, for preparing P3BT film with extremely slow evaporation rate, the solution was cast onto the substrate which was placed in a closed jar with drops of $CHCl_3$ in the bottom. By such sampling method, it took ca. 24 h for the film to be dried. The illustration for the preparation process is depicted in Scheme 3. For comparison, solution cast film with fast solvent evaporation rate in an open container without lid was also prepared. All samples were further dried under vacuum at room temperature for 12 h to remove the residual solvent prior to characterizations. The as-prepared films thickness is about 20 μm.

2.2. Characterizations. DSC measurement of the as-prepared films and annealed one was performed on a TA Q20 calorimeter system over a temperature range from −50 to 300 °C under a nitrogen gas flow at a rate of 50 mL min^{-1}. Both the heating and cooling rates were set to 10 °C/min.

Wide-angle X-ray diffraction (WAXD) measurement was conducted on a high-resolution four-circle diffractometer with rotating-anode X-ray generator (SLX-2000 & UltraX, Rigaku Co., Ltd., X-ray wavelength = 0.154 05 nm). The size of the incident beam was defined by a collimator with diameter of 2 mm. A soller slit was placed before a scintillation detector to collimate the scattered beam. The fixing time for data collection was 50 s per step, and the angular interval was 0.01°. The diffraction was recorded at a $\theta-2\theta$ symmetry scanning mode with scan angle 2θ within the range of 5°−20°.

FTIR spectra were measured with a Bruker tensor 27 spectrometer equipped with a DTGs detector. The normal transmission mode was employed for IR measurement. The spectra were obtained by coadding 16 scans at a 2 cm^{-1} resolution. For studying the thermal behavior of rr-P3BT via *in situ* FTIR, the drop-cast film on KBr plate was set on a Harrick variable temperature cell, which was placed into sample compartment of the spectrometer. Subsequently, the sample was heated at 2 °C/min from room temperature to 260 °C in a nitrogen atmosphere. During the heating process, FTIR spectra of the specimen were recorded at a 1 min interval. The IR spectra displayed here were not smoothed except for the baseline correction.

The intensity of IR bands was calculated automatically by a numerical data processor program for vibration spectroscopy, Spina Version 3, which was developed by Yukiteru Katsumoto in the Ozaki Group of Kwansei-Gakuin University. Before the intensity calculation, all of the spectra were baseline corrected. Then, peak heights were calculated at the fixed wavenumber for all spectra by this program.

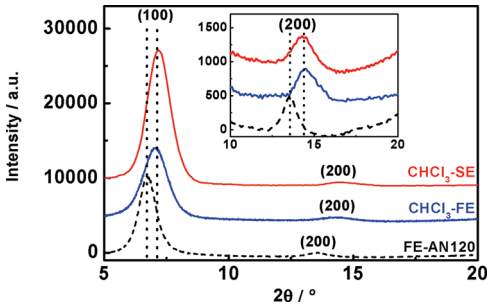

Figure 1. WAXD profiles measured at room temperature for as-cast P3BT film from chloroform solution (denoted as "$CHCl_3$-FE") and the one obtained with extremely slow solvent evaporation rate (denoted as "$CHCl_3$-SE"). The WAXD profile of the annealed sample (as-cast film annealed at 120 °C for 1 h) (denoted as "FE-AN120") is also included for comparison. Inset: the enlarged (200) diffraction peak.

3. RESULTS AND DISCUSSION

3.1. Initial Crystal Structures of P3BT Solution Cast Films Prepared with Different Solvent Evaporation Rate Investigated by WAXD. Usually, the structural ordering and the overall crystallinity in solution cast polymer film are thought to be improved by controlling the solvent evaporation rate or taking the subsequently thermal/solvent annealing treatment.[18,20,21] However, it should be noted that the crystal modifications or crystal structure may be also affected by these various sampling procedures.[11,19] For clarifying this point, we therefore prepared several P3BT films by different methods. In Figure 1, the WAXD profiles of the as-cast P3BT film from chloroform ($CHCl_3$) solution (denoted as "$CHCl_3$-FE"), the one obtained with extremely slow solvent evaporation rate (denoted as "$CHCl_3$-SE"), and the annealed one (as-cast film annealed at 120 °C for 1 h) (denoted as "FE-AN120") are compared. All of these data are measured at room temperature so that temperature factor can be precluded.

It can be seen that all samples exhibit the typical (100) and (200) diffraction peaks of P3BT. The (100) diffraction peaks are located at almost the same 2θ angles for the samples "$CHCl_3$-SE" and "$CHCl_3$-FE" although there is a subtle difference between them, whereas the smaller 2θ angle of the annealed one can be observed obviously. It means that the d_{100} spacing of the sample "FE-AN120" derived from the (100) diffraction peak is obviously larger than those of "$CHCl_3$-SE" and "$CHCl_3$-FE". According to the packing model of P3AT suggested by Prosa et al., the d_{100} spacing is defined to be associated with the interlayer distance of adjacent backbones in the *a* direction; that is, it is equal to the *a*-axis length of P3BT crystal.[17] Various crystal modifications of P3BT have been proposed based on the differences in this value. For example, it has been reported that the d_{100} spacing of P3BT form I and form II are 13.1 Å[10] and 9.6 Å,[11] respectively. Recently, Arosio and co-workers found another crystal modification, named as form I′, which demonstrates a smaller d_{100} value (d_{100} = 12.5 Å) than that of form I.[13]

In order to obtain the more accurate d_{100} spacing or the *a*-axis length of P3BT, the (200) diffraction peaks at high angle were used to perform the calculation. As shown in the inset of Figure 1, the (200) diffraction peaks of the samples "$CHCl_3$-SE", "$CHCl_3$-FE", and "FE-AN120" are respectively located at 2θ = 14.6° (d_{100} = 12.2 Å), 2θ = 14.5° (d_{100} = 12.2 Å), and 2θ = 13.6° (d_{100} = 13.0 Å). By comparing the d_{100} spacing calculated from the (200) diffraction peaks with the value mentioned above for various crystal modifications of P3BT, we could find that the d_{100} spacing of the sample "FE-AN120" is identical to that of the form I crystal (d_{100} = 13.1 Å). However, independent of the solvent evaporation rate, the d_{100} spacing of the as-cast samples "$CHCl_3$-SE" and "$CHCl_3$-FE" are both highly close to the reported value of the form I′ crystal (d_{100} = 12.5 Å) by Arosio et al.[14] Therefore, it can be concluded that the crystal modifications of P3BT solution cast films belong to form I′, whereas the annealed one takes the form I modification. The difference in crystal modification between the solution cast films and the annealed one suggests that thermal annealing will modify the crystal structure of the as cast films. In order to understand the origin of this phenomenon, we further investigated temperature-dependent phase behavior for these solution cast films.

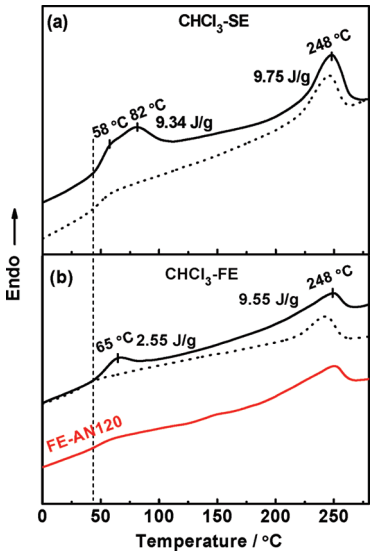

Figure 2. DSC first (solid black line) and second (dotted line) heating curves of the P3BT samples "$CHCl_3$-SE" (a) and "$CHCl_3$-FE" (b). The first heating curve of the annealed "$CHCl_3$-FE" sample is shown by the solid red line in (b).

3.2. Thermal Behavior of P3BT Cast Films Prepared with Different Solvent Evaporation Rate. Figures 2a and 2b show the first heating traces of the solution cast samples of "$CHCl_3$-SE" and "$CHCl_3$-FE", respectively. In the heating process of the two samples, it is interesting to find a similar but not identical endothermic behavior in the region of 45−100 °C. Specifically, although the endothermic behavior starts to occur from 45 °C (guided by the dashed line in Figure 2) for both the samples, the double endothermic peaks respectively centered at 58 and 82 °C can be observed clearly for the sample "$CHCl_3$-SE", whereas only a single endothermic peak located at 65 °C is identified for the sample "$CHCl_3$-FE". Moreover, the endothermic enthalpy in the temperature region of 45−100 °C increases from 2.55 to 9.34 J/g with increasing the solvent evaporation time. Because the endothermic behavior of P3BT film cast from $CHCl_3$ solution appeared in this temperature region has been reported to associated with the form I′ to form I transition,[14] the DSC results reported here indicate that the overall crystallinity and the resulting thermal stability of P3BT form I′ modification are improved greatly by controlling the solvent evaporation rate. Upon further heating, the endothermic peaks located around 248 °C ($\Delta H \approx 10$ J/g) are shown for both samples, which should be related to the melting of the P3BT form I.[14,22]

dx.doi.org/10.1021/ma200945j |*Macromolecules* 2011, 44, 6128–6135

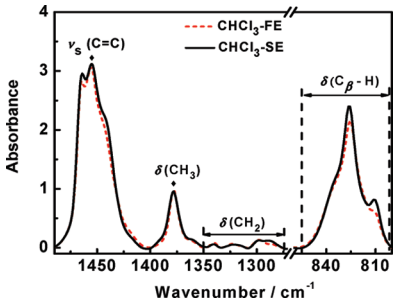

Figure 3. IR spectra measured at room temperature for the P3BT films prepared with different solvent evaporation rate in the region of 1490−800 cm^{-1}. The band at 1378 cm^{-1} is used as the normalized band.

Table 1. Band Assignment for the Physical Structure of rr-P3BT in the Region of 1490−800 cm^{-1}

IR frequency (cm^{-1})	assignment	related physical structure
1454	ν_s(C═C)	effective conjugation length[a]
1378	$\delta(CH_3)$	
1340	$\gamma(CH_2)$	butyl side chain gtt[a]
1298	$\gamma(CH_2)$	butyl side chain ttt[a]
836		amorphous phase[b]
825		form I′ crystal[b]
820	$\delta(C_\beta-H)$	high-temperature form I[b]
810		form I′ crystal[b]

[a]Assignments based on the report of references. [b]Our tentative assignment based on our WAXD and IR data.

It should be noted that in the second heating traces of DSC for both the samples (shown in Figure 2) and in the first DSC heating curve of the annealed P3BT film (shown in Figure 2b) there are no endothermic peaks in the region of 45−100 °C. Only the melting of P3BT crystal can be observed in the high temperature region. It therefore indicates that the annealed $CHCl_3$-FE film and the melt-crystallized samples take the same form I modifications.

Combining the DSC and WAXD data, we can make the conclusion that the higher crystallinity of P3BT form I′ crystal can be obtained by prolonging the solvent evaporation time. Furthermore, the form I′ to form I transition is completed at temperature above 100 °C. However, it is strange to find that the low-temperature phase transition behavior of solution cast P3BT films is obviously dependent on the solvent evaporation rate, whereas the crystal modification is not dependent on it as evidenced by the previous WAXD data. Usually the double endothermic behavior is associated with the structural changes at different levels or the melt-induced structural rearrangement process. It should be mentioned that the single endothermic behavior of P3BT film around 65 °C has been investigated by Yazawa et al.[22] and Arosio et al.[14] However, to the best of our knowledge, the double endothermic behavior of P3BT in the low-temperature region has not been reported yet. Therefore, for clarifying the concrete structure changes corresponding to the low-temperature double endothermic behavior of "$CHCl_3$-FE", the temperature-dependent IR measurements were performed.

3.3. Phase Transition of P3BT Film with High Crystallinity Investigated by Temperature-Dependent Infrared Spectroscopy. The utility of infrared spectroscopy stems from its specificity to different molecular groups and segmental constituents of polymer systems, which gives this method a unique capacity to elucidate the molecular origin of phase transition phenomena. In this work, FTIR was employed to explain the origin of the double endothermic behavior of the sample "$CHCl_3$-SE" occurred in the region of 45−100 °C. Prior to analyzing the temperature-dependent IR spectra, it is necessary to figure out the characteristic bands, which can provide the structural information on P3BT.

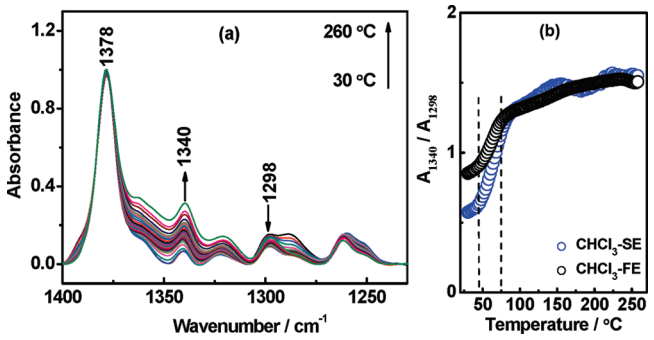

Figure 4. (a) Temperature-dependent IR spectra displayed at 10 °C intervals in the CH_2 wagging vibration region for the sample "$CHCl_3$-SE". All of the spectra are normalized by the band at 1378 cm^{-1}. (b) Relative intensity changes of the conformation-sensitive bands of butyl side chains at 1340 (G) and 1298 cm^{-1} (T) as a function of temperature for the P3BT samples "$CHCl_3$-SE" and "$CHCl_3$-FE".

Figure 3 shows the IR spectra of the samples "$CHCl_3$-SE" and "$CHCl_3$-FE" (for comparison) measured at room temperature. The spectra have been normalized to the intensity of the methyl deformation mode at 1378 cm^{-1}, which is used sometimes as the internal standard because the frequency and intensity of this vibration mode is not sensitive to the structural changes.[23] Both samples exhibit quite similar spectral profile except that some bands are larger in intensity for sample "$CHCl_3$-SE" than that for "$CHCl_3$-FE", which can be attributed to the improved crystallinity. The assignments of most of the characteristic bands for P3BT have been reported in the literature.[24−27] As listed in Table 1, the CH_2 wagging bands in the 1350−1250 cm^{-1} region are associated with the butyl side chain,[24,25] whereas the C═C stretching vibration mode in the 1480−1420 cm^{-1} region is related to the P3BT backbones.[26] The out-of-plane deformation modes of thiophene C_β−H in the 850−800 cm^{-1} region are attributed to the $\pi-\pi$ stacking of the planar backbones in the *b* direction.[27] In this spectral region, both samples demonstrate several overlapped characteristic bands, for example the bands at 810, 825, and 836 cm^{-1}. As denoted in Table 1, the bands in this region are associated with the various phases of P3BT, which will be discussed later.

Structural Change Associated with Butyl Side Chains. Figure 4 shows the bands sensitive to the butyl side chain conformation of the sample "$CHCl_3$-SE" in the region of 1350−1250 cm^{-1}, in which the bands at 1340 and 1298 cm^{-1} are respectively used to monitor the relative population of the gauche and trans conformation because they are relatively stronger in intensity and not overlapped with other bands seriously. As shown in Figure 4a, the intensity of the band at 1298 cm^{-1} (*T*) decreases whereas that of the 1340 cm^{-1} (*G*) band increases upon heating. Exchange between the trans and gauche bands indicates that the butyl side

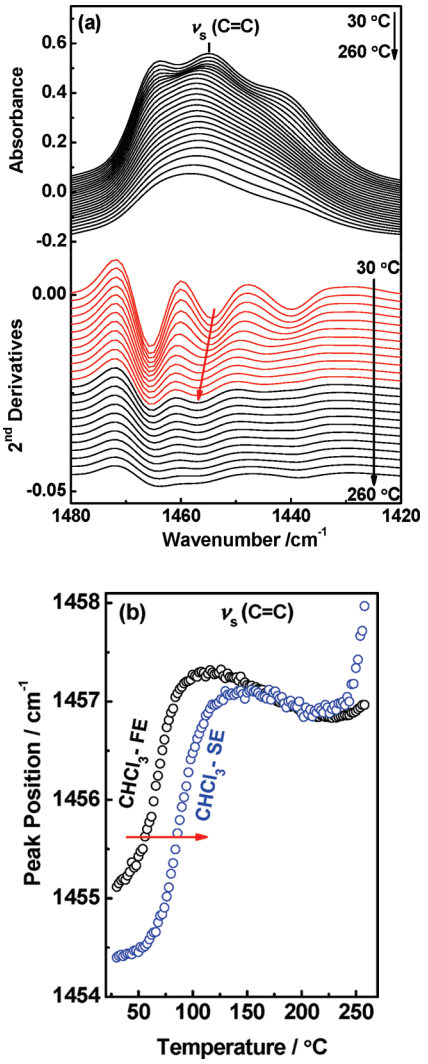

Figure 5. (a) IR spectral changes of the P3BT sample "$CHCl_3$-SE" in the 1480−1420 cm^{-1} region from 30 to 260 at 10 °C intervals and the corresponding second derivatives curves are shown in the up and down part, respectively. (b) Band shifting of the ν(C═C) mode as a function of temperature for the P3BT films prepared with different solvent evaporation rate.

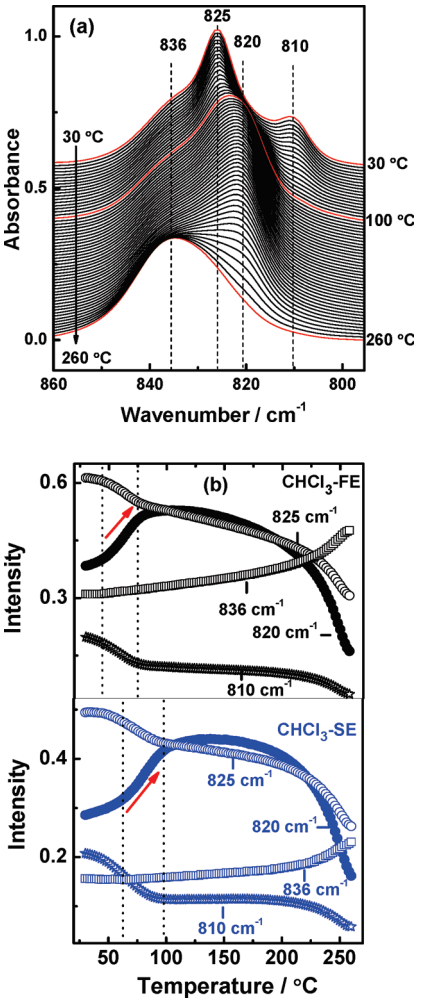

Figure 6. (a) Temperature-dependent IR spectra of the sample "$CHCl_3$-SE" displayed in a stacked way at 4 °C intervals in the C_β−H out-of-plane deformation band region. (b) Original intensity changes of the various bands as a function of temperature for the C_β−H out-of-plane deformation mode of P3BT films prepared with different solvent evaporation rate.

chains experience the conformational disordering with temperature rising.

The intensity ratio of the two conformation-sensitive bands as a function of temperature is plotted in the Figure 4b. In this way, conformational evolution of the butyl side chain could be clarified more strictly. The value of A_{1340}/A_{1298} as a function of temperature for the sample "$CHCl_3$-FE" is also included for comparison. In the heating process, abrupt intensity ratio changes of A_{1340}/A_{1298} for both samples occur in the temperature region of 45−75 °C. It indicates the butyl side chains experience the conformation-disordered transition in the same temperature region independent of the solvent evaporation rate. What should be noticed is that the initial temperature of this transition is highly in agreement with that of the endothermic peaks shown in Figure 2. With further increasing the temperature above 75 °C, almost no trans-to-gauche conformational exchange can be observed.

Structural Change Associated with Backbones. Figure 5a displays the temperature-dependent spectral change of the sample "$CHCl_3$-SE" in the 1480−1420 cm^{-1} region. The peak position of the ν_s(C═C) mode around 1454 cm^{-1} in this region has been observed to be dependent on the effective conjugation length (ECL) of P3AT, which shifts to higher wavenumber with the decrease of ECL.[28] For identifying the accurate peak positions of this band among the overlapped spectral profiles, the corresponding second derivatives of the original spectra are shown at the bottom of Figure 5a. In the second-derivative spectra, it can be clearly seen that the peak position of the ν_s(C═C) mode shifts to higher wavenumber upon heating. The quantitative result of the peak position of the ν_s(C═C) as a function of temperature for the samples "$CHCl_3$-FE" and "$CHCl_3$-SE" are depicted in Figure 5b. Upon heating, it is found that the ν_s(C═C) mode shows abrupt high-wavenumber shifting in two temperature regions for both samples. The first one occurs in the temperature range of 45−100 °C, which are associated with the low-temperature endothermic behavior shown in Figure 2. The second one is in the melting temperature region

dx.doi.org/10.1021/ma200945j |*Macromolecules* 2011, 44, 6128–6135

(220−260 °C) of the P3BT crystal. Undoubtedly, the high-wavenumber shifting of ν_s(C═C) in the melting temperature region is caused by the disordering of the conjugated backbone. Therefore, the high-wavenumber shifting of ν_s(C═C) in the low-temperature region also suggests that there is the destruction of backbone planarity, that is, the decreasing in ECL with heating. Compared with sample "$CHCl_3$-FE", it is clearly revealed that the disordering of the conjugated backbone in "$CHCl_3$-SE" appears in the higher temperature region, which suggests that the conjugated chain in "$CHCl_3$-SE" is more stable.

Structural Change Associated with π−π Stacking. Figure 6a shows temperature-dependent spectral changes of thiophene C_β−H out-of-plane deformation modes ($\delta(C_\beta-H)$) for the sample "$CHCl_3$-SE" in the region of 850−800 cm^{-1}, in which the bands are related to the π−π stacking of planar backbones in the *b* direction as mentioned. Clearly, four bands located at 810, 820, 825, and 836 cm^{-1} can be identified in this spectral range with heating. Among these bands, the band at 836 cm^{-1} should be assigned to the amorphous band because of its domination at 260 °C in which P3BT is in the molten state. On the basis of the previous WAXD result in Figure 1, the bands at 810 and 825 cm^{-1} which appear in the spectrum measured at room temperature are tentatively assigned to the P3BT form I′. According to the report by Arosio's group, form I modification of P3BT is stable above 100 °C,[14] in which the 820 cm^{-1} band is dominated as shown in Figure 6a. Therefore, it is reasonable to make the conclusion that the 820 cm^{-1} band is the characteristic band of P3BT form I modification at high temperature.

The intensity changes of the δ (C_β−H) mode in the whole heating process for the P3BT films prepared with different solvent evaporation rate are compared in Figure 6b. For the sample "$CHCl_3$-FE", the characteristic bands at 810 and 825 cm^{-1} for P3BT form I′ decreases simultaneously in intensities whereas the intensity of the 820 cm^{-1} band related to form I increases in the region of 50−75 °C. It suggests that the endothermic peak around 65 °C (shown in Figure 2b) is related to the form I′ to form I phase transition. With increasing temperature from 220 to 260 °C, the transformation of the 820 cm^{-1} band to the amorphous band at 836 cm^{-1} is attributed to the melting of the form I crystal to the amorphous phase. Similar spectral observation can be found for "$CHCl_3$-SE" except that the temperature region of form I′ to form I phase transition is obviously delayed and shifts to higher temperature (60−100 °C) compared to that of "$CHCl_3$-FE". For both cases, it is noted that the intensity of the 836 cm^{-1} band is stable and unchanged, which indicates that form I′ to form I phase transition belongs to the solid-to-solid phase transition.

3.4. Effect of Solvent Evaporation Rate on Order-to-Disorder Structural Transition of P3BT Solution Cast Films. The above spectral results show that the P3BT films prepared with different solvent evaporation rate exhibit similarly structural changes in the low temperature region (45−100 °C), which could be described in several aspects. First, butyl side chains experience the "melting" process through the exchange between trans and gauche conformation. Second, the conformational disordering of the coplanar thiophene ring occurs, which leads to the decreasing of ECL upon heating. Third, the π−π stacking mode in the crystalline phase is also changed with increasing temperature. These observations together with the DSC data (shown in Figure 2) strongly indicate that there are the order-to-disorder phase transitions corresponding to the low-temperature endothermic behavior for P3BT solution cast films prepared with various solvent evaporation rates. Our previous WAXD data suggests that both samples "$CHCl_3$-FE" and "$CHCl_3$-SE" demonstrate the same crystal modification (form I′) at the initial state and the high-temperature annealed P3BT samples usually take the form I modification. Therefore, it is rational to assign the order-to-disorder phase transitions observed in the low temperature region to the form I′ to form I transition.

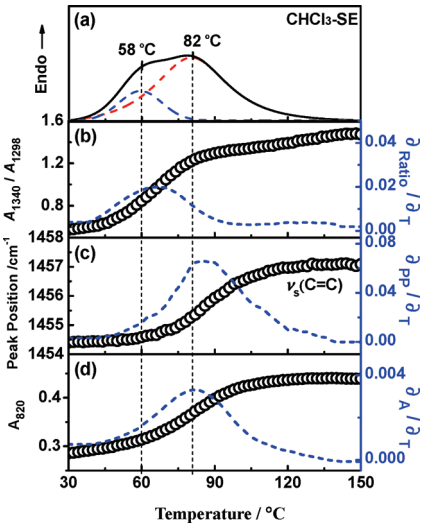

Figure 7. DSC heating trace (a) and the spectral changes associated with butyl side chain characterized by A_{1340}/A_{1298} (b), conjugated chain length characterized by peak position of ν_s (C═C) (c), and π−π stacking mode characterized by A_{820} (d) in the low-temperature region as a function of temperature for P3BT "$CHCl_3$-SE". The corresponding first derivate curves of the spectral changes in (b)−(d) are also included with dashed lines.

On the basis of the IR and DSC results, it is interested to find that the conformational disordering of the butyl side chains and the backbones occurs around 65 °C simultaneously during the phase transition process for the sample prepared with fast solvent evaporation rate (that is, the sample "$CHCl_3$-FE"). However, for the solution cast film prepared with slow solvent evaporation rate (that is, the sample "$CHCl_3$-SE"), it seems that there are the sequential structure changes of the butyl side chains and the backbones during the heating process. For investigating the sequentially structural changes in detail, the DSC curve of "$CHCl_3$-SE" and the corresponding spectral changes associated with butyl side chain, conjugated chain length, and π−π stacking mode in the low-temperature region are plotted together for comparison in Figure 7.

As shown in Figure 7a, the DSC curve of P3BT sample "$CHCl_3$-SE" exhibits the double endothermic peaks located at 58 and 82 °C, which has been mentioned previously. Figure 7b shows that the intensity ratio of A_{1340}/A_{1298} increases significantly in the region of 45−75 °C. On the basis of the discussion in section 3.3, it indicates the side chains experience the order-to-disorder conformational transition. The first derivative of the A_{1340}/A_{1298} as a function of temperature further indicates that the trans-to-gauche conformational exchange of butyl side chains occurs most drastically around 60 °C. This temperature is very close to that of the first endothermic peak located at 58 °C, the appearance of which can be accordingly assigned to the "melting" of P3BT side chains.[17,25,29,30]

Figures 7c and 7d respectively show the wavenumber shifting of the ν_s(C═C) mode and the intensity change of the band at

dx.doi.org/10.1021/ma200945j |*Macromolecules* 2011, 44, 6128–6135

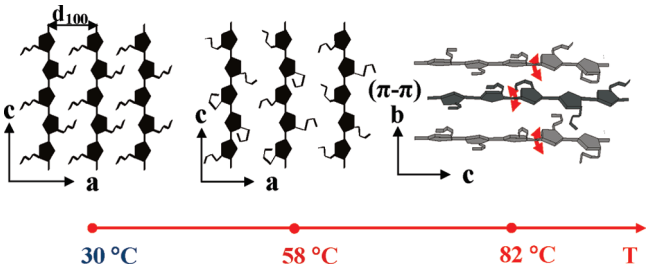

Figure 8. Schematic illustration of the structural changes related to the double endothermic behavior in the region of 30−100 °C for P3BT sample "$CHCl_3$-SE".

820 cm^{-1} in the low-temperature region, which have been used to monitor the changes in the ECL and the $\pi-\pi$ stacking mode during the process of phase transition. It is found that the abrupt change of the $\pi-\pi$ stacking mode occurs almost in the same temperature region as the conformational disordering of P3BT backbones. Furthermore, according to the first derivative curves of the ν_s(C═C) peak position and the A_{820} as a function of temperature, the maximum change rate as depicted in Figures 7c and 7d both lie around 82 °C, the temperature of which is equal to that of the second endothermic peak as shown in Figure 7a. This result clarifies that the endothermic behavior occurred at 82 °C is associated with the destruction of the backbone's coplanarity, which may be induced by the twisting of the conjugated backbones, as well as with the disordering of the $\pi-\pi$ stacking modes.

In summary, the structural disordering in a sequential way for butyl side chain and conjugated backbone can be clearly revealed in Figure 7. It should be the reason for the double endothermic behavior of P3BT sample "$CHCl_3$-SE". A schematic illustration of the sequential structure changes corresponding to the double endothermic behavior of P3BT is depicted in Figure 8. However, as suggested by the WAXD data shown in Figure 1, both P3BT samples "$CHCl_3$-SE" and "$CHCl_3$-FE" take the form I′ crystal modification at room temperature, which is not affected by the solvent evaporation rate. If so, why do they demonstrate the different form I′ to form I phase transition behavior during the subsequent heating process?

By examining the spectral difference of "$CHCl_3$-SE" and "$CHCl_3$-FE" at room temperature in detail, it can be found that the P3BT crystal structure of solution cast film is actually affected by the solvent evaporation rate although its *a*-axis length is almost unchanged as evidenced by the WAXD data. First, as shown in the Figure 4b, the initially smaller intensity rate of A_{1340}/A_{1298} for "$CHCl_3$-SE" than that for "$CHCl_3$-FE" represents the higher concentration of trans-butyl content in "$CHCl_3$-SE". Second, the initial peak position of the ν_s(C═C) mode for "$CHCl_3$-SE" is a little lower than that for "$CHCl_3$-FE" as displayed in Figure 5b, which suggests that the effective conjugation length is increased by prolonging the solvent evaporation time.

It should be noted that the increasing trans-butyl content in "$CHCl_3$-SE" could not improve the "melting temperature" of the butyl side chains. Therefore, the endothermic behaviors start to occur from 45 °C (guided by the dashed line in Figure 2) for both samples. However, the more ordered conformation of P3BT backbones or the increasing effective conjugated chain length may increase the lamellar thickness of P3BT form I′ crystal. Therefore, the thermal stability of P3BT form I′ crystal in "$CHCl_3$-SE" is accordingly improved by controlling the solvent evaporation rate. Furthermore, the order-to-disorder transition related to the backbone and the $\pi-\pi$ stacking mode appears at higher temperature.

4. CONCLUSION

In the present work, the effect of solvent evaporation rate on the condensed structure and the order-to-disorder phase transition of rr-P3BT solution cast film were investigated by DSC, WAXD, and FTIR. WAXD data show that P3BT crystal takes the same form I′ modification independent of the solvent evaporation rate. However, the spectral results suggest that, except for the improvement in crystallinity, the regularity of the butyl side chains and the effective conjugation length of backbones can also be improved by prolonging the solvent evaporation time, which lead to the distinct double endothermic behavior in the low-temperature region for the P3BT sample prepared with slow solvent evaporation rate.

By temperature-dependent IR spectroscopy, the spectral changes of several characteristic bands associated with the butyl side chains, conjugated backbones, and $\pi-\pi$ stacking modes of P3BT solution cast films were *in situ* monitored. It is found that there is a disorder-to-order structural transition in the low-temperature region (ca. 65 °C), which can be assigned to the phase transition from form I′ to form I. Both IR and DSC results show that such order-to-disorder phase transitional behavior is largely affected by the solvent evaporation rate. That is, synchronized or sequential structural transition of the butyl side chains and conjugated backbones can be observed for P3BT samples respectively prepared with fast and slow solvent evaporation rate. Our spectral analysis suggest that the disordering of the side-chain packing or "melting" is assigned for the endothermic behavior around 58 °C, which is not affected by the solvent evaporation rate. However, the destruction of the backbone coplanarity and the disordering of the $\pi-\pi$ stacking move to the higher temperature region with prolonging the solvent evaporation time, which contribute to the endothermic peak around 82 °C. The origin of this higher thermal stability for the P3BT sample prepared with slow solvent evaporation rate is explained by the increased effective conjugation length or lamellar thickness of P3BT. Our results clearly demonstrate that the condensed structures of P3BT solution cast films are affected not only by the evaporation rate but also by the subsequently thermal annealing process.

AUTHOR INFORMATION

Corresponding Author

*Fax: +86-532-84022791. E-mail: zjm@qust.edu.cn.

ACKNOWLEDGMENT

The financial support from Taishan Mountain Scholar Constructive Engineering Foundation (TS20081120), Doctoral Fund of Qingdao University of Science and Technology and Natural Science Fund for Distinguished Young Scholars of Shandong Province (JQ200905) are greatly appreciated. The authors thank Prof. Christoph Bubeck for helpful discussions. Jianming Zhang thanks the Alexander von Humboldt foundation for supporting his research stay at the Max Planck Institute for Polymer Research in Mainz, Germany.

REFERENCES

(1) Bert de, Boer; Facchetti, A. *Polym. Rev.* **2008**, *48*, 423–431.
(2) Sirringhaus, H.; Ando, M. *MRS Bull.* **2008**, *33*, 676–682.
(3) Roncali, J. *Chem. Rev.* **1992**, *92*, 711–738.
(4) McCullough, R. D.; Ewbank, P. C. In *Handbook of Conducting Polymers*, 2nd ed.; Skotheim, T. A., Elsenbaumer, R. L., Renolds, J. R., Eds.; Marcel Dekker: New York, 1998; p 225.
(5) Mennon, R.; Yoon, C. O.; Moses, D.; Heeger, A. J. In *Handbook of Conducting Polymers*, 2nd ed.; Skotheim, T. A., Elsenbaumer, R. L., Renolds, J. R., Eds.; Marcel Dekker: New York, 1998; p 27.
(6) He, M.; Zhao, L.; Wang, J.; Han, W.; Yang, Y.; Qiu, F.; Lin, Z. *ACS Nano* **2010**, *4*, 3241–3247.
(7) Byun, M.; Laskowski, R. L.; He, M.; Qiu, F.; Jeffries-EL, M.; Lin, Z. *Soft Matter* **2009**, *5*, 1583–1586.
(8) Xu, J.; Wang, J.; Mitchell, M.; Mukherjee, P.; Jeffries-EL, M.; Petrich, J. W.; Lin, Z. *J. Am. Chem. Soc.* **2007**, *129*, 12828–12833.
(9) Dennler, G.; Sariciftci, N. S.; Brabec, C. Conjugated Polymer Based Organic Solar Cells. In *Semiconducting Polymers: Chemistry, Physics and Engineering*, 2nd ed.; Hadzioannou, G., Malliaras, G. G., Eds.; Wiley-VCH: Weinheim, 2006; Vol. 1.
(10) Causin, V.; Marega, C.; Marigo, A. *Macromolecules* **2005**, *38*, 409–415.
(11) Lu, G. H.; Li, L. G.; Yang, X. N. *Adv. Mater.* **2007**, *19*, 3594–3598.
(12) Lu, G. H.; Li, L. G.; Yang, X. N. *Macromolecules* **2008**, *41*, 2062–2070.
(13) Buono, A.; Son, N. H.; Raos, G.; Gila, L.; Cominetti, A.; Catellani, M.; Meille, S. V. *Macromolecules* **2010**, *43*, 6772–6781.
(14) Arosio, P.; Moreno, M.; Famulari, A.; Raos, G.; Catellani, M.; Meille, S. V. *Chem. Mater.* **2009**, *21*, 78–87.
(15) Joshi, S.; Grigorian, S.; Pietsch, U.; Pingel, P.; Zen, A.; Neher, D.; Scherf, U. *Macromolecules* **2008**, *41*, 6800–6808.
(16) Wu, Z. Y.; Petzold, A.; Henze, T.; Albrecht, T. T.; Lohwasser, R. H.; Sommer, M.; Thelakkat, M. *Macromolecules* **2010**, *43*, 4646–4653.
(17) Prosa, T. J.; Winokur, M. J. *Macromolecules* **1996**, *29*, 3654–3656.
(18) Gurau, M. C.; Delongchamp, D. M.; Vogel, B. M.; Lin, E. K.; Fischer, D. A.; Sambasivan, S.; Richter, L. J. *Langmuir* **2007**, *23*, 834–842.
(19) Yang, H.; Shin, T. J.; Yang, L.; Cho, K.; Ryu, C. Y.; Bao, Z. *Adv. Funct. Mater.* **2005**, *15*, 671–676.
(20) Li, G.; Shrotriya, V.; Huang, J.; Yao, Y.; Moriarty, T.; Emery, K.; Yang, Y. *Nature Mater.* **2005**, *4*, 864–868.
(21) Ho, P. K.-H.; Chua, L.-L.; Dipankar, M.; Gao, X.; Qi, D.; Wee, A. T.-S.; Chang, J.-F.; Friend, R. H. *Adv. Mater.* **2007**, *19*, 215–221.
(22) Yazawa, K.; Inoue, Y.; Yamamoto, T.; Asakawa, N. *Phys. Rev. B* **2006**, *74*, 094204–1−12.
(23) Zerbi, G.; Chierichetti, B.; Ingänas, O. *J. Chem. Phys.* **1991**, *94*, 4646–4658.
(24) Curtis, M. D.; Nanos, J. I.; Moon, H.; Jahng, W. S. *J. Am. Chem. Soc.* **2007**, *129*, 15072–15084.
(25) Tashiro, K.; Ono, K.; Mipagawa, Y.; Kobayashi, M.; Kawai, T.; Yoshino, Y. *J. Polym. Sci., Part B: Polym. Phys.* **1991**, *29*, 1223–1233.
(26) Qiao, X. Y.; Wang, X. H.; Mo, Z. S. *Synth. Met.* **2001**, *118*, 89–95.
(27) Winokur, M. J.; Spiegel, D.; Kim, Y.; Hotta, S.; Heeger, A. J. *Synth. Met.* **1989**, *28*, 419–426.
(28) Botta, C.; Luzzati, S.; Bolognesi, A.; Catellani, M.; Destri, S.; Tubino, R. *Mater. Res. Soc. Symp. Proc.* **1990**, *137*, 397–406.
(29) Prosa, T. J.; Winokur, M. J.; Moulton, J.; Smith, P.; Heeger, A. J. *Macromolecules* **1992**, *25*, 4364–4372.
(30) Meille, S. V.; Romita, V.; Caronna, T.; Lovinger, A. J.; Catellani, M.; Belobrzeckaja, L. *Macromolecules* **1997**, *30*, 7898–7905.